Measurement of the Positive Muon Lifetime and Determination of the Fermi Constant to Part-per-Million Precision

D. M. Webber,[1] V. Tishchenko,[2] Q. Peng,[3] S. Battu,[2] R. M. Carey,[3] D. B. Chitwood,[1] J. Crnkovic,[1] P. T. Debevec,[1] S. Dhamija,[2] W. Earle,[3] A. Gafarov,[3] K. Giovanetti,[4] T. P. Gorringe,[2] F. E. Gray,[5] Z. Hartwig,[3] D. W. Hertzog,[1] B. Johnson,[6] P. Kammel,[1] B. Kiburg,[1] S. Kizilgul,[1] J. Kunkle,[1] B. Lauss,[7] I. Logashenko,[3] K. R. Lynch,[3] R. McNabb,[1] J. P. Miller,[3] F. Mulhauser,[1,7] C. J. G. Onderwater,[1,8] J. Phillips,[3] S. Rath,[2] B. L. Roberts,[3] P. Winter,[1] and B. Wolfe[1]

(MuLan Collaboration)

[1]*Department of Physics, University of Illinois at Urbana-Champaign, Urbana, Illinois 61801, USA*
[2]*Department of Physics and Astronomy, University of Kentucky, Lexington, Kentucky 40506, USA*
[3]*Department of Physics, Boston University, Boston, Massachusetts 02215, USA*
[4]*Department of Physics, James Madison University, Harrisonburg, Virginia 22807, USA*
[5]*Department of Physics and Computational Science, Regis University, Denver, Colorado 80221, USA*
[6]*Department of Mathematics and Physics, Kentucky Wesleyan College, Owensboro, Kentucky 42301, USA*
[7]*Paul Scherrer Institute, CH-5232 Villigen PSI, Switzerland*
[8]*KVI, University of Groningen, NL-9747AA Groningen, The Netherlands*

(Received 5 October 2010; published 25 January 2011; corrected 7 February 2011)

We report a measurement of the positive muon lifetime to a precision of 1.0 ppm; it is the most precise particle lifetime ever measured. The experiment used a time-structured, low-energy muon beam and a segmented plastic scintillator array to record more than 2×10^{12} decays. Two different stopping target configurations were employed in independent data-taking periods. The combined results give $\tau_{\mu^+}(\mathrm{MuLan}) = 2\,196\,980.3(2.2)$ ps, more than 15 times as precise as any previous experiment. The muon lifetime gives the most precise value for the Fermi constant: $G_F(\mathrm{MuLan}) = 1.166\,378\,8(7) \times 10^{-5}$ GeV^{-2} (0.6 ppm). It is also used to extract the $\mu^- p$ singlet capture rate, which determines the proton's weak induced pseudoscalar coupling g_P.

DOI: 10.1103/PhysRevLett.106.041803 PACS numbers: 14.60.Ef, 06.20.Jr, 12.15.Ji, 13.35.Bv

A measurement of the positive muon lifetime τ_{μ^+} to high precision determines the Fermi constant G_F according to the relation

$$\frac{1}{\tau_\mu} = \frac{G_F^2 m_\mu^5}{192\pi^3}(1 + \Delta q). \quad (1)$$

Here, Δq represents well-known phase space and both QED and hadronic radiative corrections [1], and we assume that G_F is universal for weak interactions. Strictly speaking, τ_{μ^+} determines a muon-decay-specific coupling, denoted G_μ, which could be compared to other G_F determinations as a test of the standard model [2].

Prior to 1999, the limitation on the precision of G_F was dominated by the uncertainty on Δq. Van Ritbergen and Stuart were the first to compute the second-order QED radiative corrections in the massless electron limit, reducing the theoretical uncertainty to below 0.3 ppm [3], and well below the then-current experimental uncertainty. This development motivated a new generation of precision muon lifetime measurements, MuLan [4] and FAST [5]. More recently, Pak and Czarnecki extended the result in Ref. [3] to finite electron mass, which shifts the predicted decay rate $1/\tau_\mu$ by -0.43 ppm; alternatively, it decreases G_F by 0.21 ppm [6].

In Ref. [4], we reported an 11 ppm measurement of τ_{μ^+} based on a relatively short commissioning run. This Letter reports the results from a 100 times larger data set, accumulated by using the final setup of the experiment.

The experiment is designed to stop muons in a target during a beam-on accumulation interval and measure the decay positrons—primarily from the $\mu^+ \to e^+ \nu_e \bar{\nu}_\mu$ decay mode—during a beam-off measurement period. The two running periods, R06 and R07, used different targets. More than 10^{12} decays were recorded in each period.

The experiment used the $\pi E3$ beam line at the Paul Scherrer Institute. During the run, positive muons from at-rest pion decay near the surface of the production target are directed to the experiment through two opposing vertical dipole magnets and a series of 15 magnetic quadrupole lenses. A velocity-selecting $\vec{E} \times \vec{B}$ separator is tuned to pass muons and reject positrons. A special feature of the beam line is a custom, 60-ns switching, 25-kV kicker [7]. When energized, the electric field across the 120-mm vertical gap and 1500-mm length displaces the muon beam by 46 mm at the exit and deflects it by 45 mrad onto a downstream collimator. The muon flux of $\sim 10^7$ μ/s at the experimental focus is reduced by an extinction factor $\epsilon \sim 10^3$. The kicker is switched by an external timing

circuit that synchronizes the data collection cycles into 5 μs kicker-off accumulation periods T_A followed by 22 μs kicker-on measurement periods T_M, also called "fills." The kicker voltage stability during the measuring period $V(t)$, coupled with the derivative $d\epsilon/dV(t)$ at full voltage, determines the time stability of the background from this source.

Muons which arrive at the target are nearly 100% polarized. Because of parity violation in the decay, positrons are emitted preferentially in the direction of the muon spin. Any change in the ensemble-averaged residual polarization $\langle \vec{P}_\mu \rangle$ during the measuring period can result in an effective time-dependent acceptance if the individual detectors are not symmetric around the stopping target and identical in response. For many materials, the magnitude of $\langle \vec{P}_\mu \rangle$ is reduced during the muon stopping process. It can also be reduced by the application of a magnetic field transverse to the spin direction and having a field strength sufficient to precess the spin rapidly compared to T_A. In practice, a residual longitudinal polarization $\langle \vec{P}_L \rangle$ remains, owing to misalignment of the transverse field. The array of detectors is highly and symmetrically segmented. The sum of events recorded by a detector at angle (θ, ϕ) with those from an equally efficient detector at $(180° - \theta, 180° + \phi)$ form a decay histogram that is immune to changes in $\langle \vec{P}_\mu \rangle$.

Several differences compared to the setup used in Ref. [4] involve the muon delivery and the stopping target. A 200-mm-diameter vacuum beam pipe now extends the beam line through the detector array (see Fig. 1) ending in a thin Mylar window. Muons are stopped in a 21-mm horizontal by 10-mm vertical (rms) spot centered on the target disk. The R06 target is a 0.5-mm-thick, 200-mm-diameter ferromagnetic AK-3 foil [8], having an internal in-plane bulk magnetic field of approximately 0.4 T. The R07 target is a 2-mm-thick, 130-mm-diameter crystalline quartz (SiO_2) disk, in which stopped muons form muonium 90% of the time [9]. A Halbach arrangement of permanent magnets provides a nearly uniform 0.013 T field in the plane of the quartz disk. The internal AK-3 magnetization or the external magnet field normally points left or right in the horizontal direction, and the muon spin precesses in the vertical plane with periods of 18 and 2.6 ns, respectively, for free muons in AK-3 or muonium in quartz. The 10% of muons in diamagnetic states in quartz precess with a period of 550 ns, which is observed. Both targets can swing open to allow the beam to pass unobstructed to a proportional wire chamber, which monitors the rate and transverse profile at the downstream end of the experiment.

The detector array consists of 170 stacked pairs of 3-mm-thick plastic scintillators. They are arranged in a truncated icosahedron geometry and grouped in 20 hexagon and 10 pentagon houses. The center of a pair of detectors is 383 mm from the target. Each scintillator is viewed by either a Photonis (PH) or Electron Tubes (ET) 29-mm photomultiplier (PMT). On average, 80 photoelectrons are registered for each minimum-ionizing particle, which yields a well-defined pulse shape from through-going decay positrons. The pulse-height distribution fit to a Landau function convoluted with a Gaussian response provides a calibration point for each detector. The most probable value is used as a relative calibration of the gain stability versus time in the experimental run and, most importantly, versus time during the measuring cycle. An LN203 nitrogen laser distributes 300-ps-long UV pulses (337 nm) to 24 of the detectors and to an externally located reference counter; this pulse excites the scintillator similarly to an ionizing particle. The asynchronous pulsing of the laser provides a sharply timed common pulse that allows for a relative time stability monitor during the measurement period and an independent confirmation of gain stability.

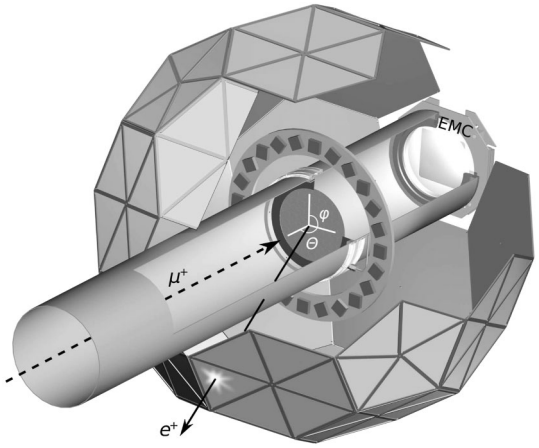

FIG. 1. Diagram of the experiment. Muons are transported to the AK-3 or quartz disk targets through a vacuum beam pipe, which is lined on the inside with 0.1-mm-thick AK-3 foils polarized in the azimuthal direction. 170 pairs of triangular scintillator detectors, each read out individually, surround the target. The Halbach magnetic ring is used only for the quartz disk. A wire chamber (EMC) is placed at the rear to monitor the beam profile when the targets are opened.

The signals from the 340 PMTs are recorded by using 450 MHz, 8-bit, waveform digitizers. Each has four independent inputs associated with the inner and outer elements of a pair of detectors and the geometrically opposite pair. The waveform digitizer sampling frequency is set by an Agilent E4400 signal generator having stability better than 0.01 ppm/month. The frequency was set to $\pm$450 ppm of 451 MHz, with the exact value unknown to the collaboration and only disclosed after the completion of a blinded analysis of the two data sets. The "clock tick" (c.t.) time units have the conversion 1 c.t. $\approx$ 2.2 ns. Normally, 24 analog-to-digital converter samples (53 ns) comprise a full waveform; they are recorded when an input signal exceeds a set threshold, with four to eight samples preceding the trigger point. The digitization is extended if the threshold is exceeded at the 24th sample. For the average pulse, the full width at 20% maximum is 9 ns.

The 130 terabytes of raw waveforms are first converted into lists of valid ''hits'' having characteristic times and energies for each detector. The waveforms are fit to pulse-shape templates, prepared from a set of low-rate events; the time of a decay is defined as the peak of the pulse shape. In more than 99.9% of the cases, a single pulse exists on a waveform and it can be identified reliably. A distribution of pulse energies is made for each detector, and a run-by-run dependent pulse threshold is established at the minimum in the distribution between the low-amplitude PMT noise and the minimum-ionizing particle peak (45%–55% of the minimum-ionizing particle peak amplitude). Rare multiple-pulse waveforms are more difficult to characterize, requiring an iterative approach that adds additional pulses as needed and/or introduces more sophisticated fitting methods. When two pulses are separated by more than 3 c.t., the procedure works well. For shorter separation times, only one hit is reconstructed and its time is set to the energy-weighted average of the analog-to-digital converter samples. For resolved pulses, an ''artificial dead time'' (ADT) can still be applied on a per-detector basis, eliminating pulses when a minimum time separates sequential hits in the same scintillator. The ADT used in the analysis varies from 5 to 68 c.t. and represents an important diagnostic of the pileup-correction procedure.

Histograms are filled with inner-outer coincident events for each detector pair; the coincidence window width is set equal to the ADT. The muon lifetime is obtained from a fit to the sum of the 170 individual histograms using the function

$$F(t) = A\exp(-t/\tau_\mu) + B, \tag{2}$$

where B accounts for the flat background. Under our running conditions, uncorrected pileup would shift the fitted lifetime from its true value by $\delta\tau_\mu/\mathrm{ADT} = 24$ ppm/c.t. Pileup is corrected by using a statistical procedure based on the data themselves. When a hit is observed at time t_i, in fill j, an interval between t_i and t_i + ADT is searched in fill $j + 1$. If a hit is observed in this interval, its time is recorded in a separate histogram, which is then added back into the original decay histogram. The process is repeated for higher-order pileup, and it includes fine adjustments to account for time jitter between inner-outer coincidences and for uncorrelated single hits and other distortions. A Monte Carlo study verified the pileup-correction procedure with input hits occurring at actual coincidence, singles, and background rates and with the measured time jitter in inner-outer hits. It was also tested at much higher rates where the correction is correspondingly larger. Pileup-related lifetime shifts are reduced to $\delta\tau_\mu/\mathrm{ADT} = +0.018$ ppm/c.t. A linear extrapolation to zero ADT gives our quoted value. The overall pileup systematic uncertainty is estimated to be less than 0.2 ppm. An alternative approach to pileup correction is to add an explicit 1st-order pileup term, $\exp(-2t/\tau_\mu)$, to the fit function in Eq. (2). This yields the same lifetime as our correction procedure but at the price of doubling the uncertainty on τ_μ, owing to the correlation of the additional term in the fit.

Because the residual polarization in the AK-3 target is small enough that it is not distinguishable in individual time spectra, Eq. (2) describes the R06 data well. A fit to the pileup-corrected event histogram, summed over all detector pairs, gives a $\chi^2/\mathrm{d.o.f.} = 1.03 \pm 0.04$ for a fit start time 220 ns into the measurement period and an ADT of 6 c.t. Although no ϕ dependence is observed for individual fits, a 12 ppm slope exists in the distribution of lifetime versus $\cos(\theta)$, which is canceled to better than 0.10 ppm by the symmetry of the detector array and the accuracy of the alignment. The slope is consistent with the relaxation of a spin component along the beam axis. The lifetimes of the 85 opposite detector pairs, which are first summed and then fit, is flat, when plotted from $\theta = 0°$ to 90°, and the distribution of results is Gaussian having a normalized width $\sigma/\mathrm{mean} = 0.90 \pm 0.08$, which is in acceptable agreement with 1.0.

In contrast, the R07 quartz data are complicated by the relatively slow precession and relaxation of the diamagnetic muons. The amplitude of the precession signal for individual detectors can be as large as 0.1%, and the longitudinal polarization can be as large as 0.15%. A different analysis procedure, which is insensitive to small and unknown efficiency differences, is used. Each detector-pair histogram is first fit by using Eq. (2) with A multiplied by $[1 + P_2\exp(-t/\tau_2)\sin(\omega t + \phi)]$; here P_2 and τ_2 are the transverse polarization and relaxation time constant, respectively. These fits result in 170 ''effective'' muon disappearance rates, which differ from the true muon decay rate because of the relaxation of the longitudinal spin component. Next, the 170 effective lifetimes are fit to extract the true muon lifetime by using a function that accounts for the position of detectors relative to the longitudinal polarization direction. This fit takes advantage of the smooth geometrical-based evolution of the relaxation effect. The leading systematic uncertainty of 0.20 ppm for this procedure is due to the uncertainty of the beam position on the target. The lifetime obtained is in agreement (to 0.3 ppm) with the result from a fit to the simple sum of detector-pair histograms using Eq. (2).

Instability of the combined detector and electronics response, or ''gain,'' during the measurement period is a possible source for a systematic error. It will result in gaining or losing hits, which can shift the fitted lifetime. Four effects were identified: (i) When triggered to begin the recording of fills, a fan-out unit induced a 1.3×10^{-4} gain oscillation in each waveform digitizer. The effect, which is reproducible in bench tests, disappears in ~ 4 μs. An empirical function is used to characterize and correct for the oscillation prior to the final fits. (ii) A short-time-scale gain shift occurs when one hit closely follows

a preceding hit. The second hit is affected by the remnant long-decay-time scintillator light from the first pulse and by the intrinsic recovery time of the PMT and voltage divider. A ~1% increase in detector gain exists following a pulse, which persists for 50 or 500 ns in PH- or ET-instrumented detectors, respectively. (iii) A long-time-scale change also exists that differs by PMT type. The PH-tube gains increase by 1.8×10^{-4}, and the ET-tube gains decrease by 5×10^{-4}, over the 22 μs measurement period. (iv) When below-threshold pulses fall in either the peak or pedestal regions of a trigger pulse, they can either raise or lower the trigger pulse amplitude, respectively. Strictly speaking, this is a pileup effect, which is not accounted for in the pileup-correction procedure.

These four phenomena are interrelated and give rise to an overall variation of 3×10^{-4} in the gain during the fill. This variation was separately evaluated for PH- and ET-instrumented detectors by using the most probable value versus time in fill and was used, after normalization and prior to the final lifetime fits, to correct for the resulting time spectrum distortion. After all corrections are applied, the shift in lifetime compared to uncorrected spectra is $+0.50 \pm 0.25$ ppm. The procedure was tested by accumulating a high-threshold spectrum, which amplifies the time spectrum distortion by roughly a factor of 60. The lifetimes derived from normal- and high-threshold settings, following the correction procedures, are in good agreement.

The complete summary of systematic uncertainties is given in Table I, including small effects related to muon stops upstream of the target, the short-term and long-term time response stability based on the laser system, and the uncertainty on the absolute clock frequency.

The stability of the result versus start time of the fit is a powerful collective diagnostic because pileup, gain stability, and spin effects all might exhibit time dependence. For both R06 and R07, the lifetime does not depend on the fit start time, apart from the statistically allowed variation. Furthermore, it does not depend on the run number or magnetic field orientation.

TABLE I. Systematic and statistical uncertainties in parts per million. The errors in different rows of the table are not correlated to each other. If only one error appears in a given row, the effect is 100% correlated between the two run periods.

Effect uncertainty in ppm	R06	R07
Kicker stability	0.20	0.07
Spin precession or relaxation	0.10	0.20
Pileup	0.20	
Gain stability	0.25	
Upstream muon stops	0.10	
Timing stability	0.12	
Clock calibration	0.03	
Total systematic	0.42	0.42
Statistical uncertainty	1.14	1.68

The final results for the two running periods are in excellent agreement:

$$\tau_\mu(\mathrm{R06}) = 2\,196\,979.9 \pm 2.5 \pm 0.9 \text{ ps},$$
$$\tau_\mu(\mathrm{R07}) = 2\,196\,981.2 \pm 3.7 \pm 0.9 \text{ ps}. \quad (3)$$

Here, the first errors are statistical and the second systematic. The comparison between R06 and R07 affirms, at the parts-per-million level, the expectation that the lifetime of bound muonium does not differ appreciably from the free lifetime [10]. Combined we obtain

$$\tau_\mu(\mathrm{MuLan}) = 2\,196\,980.3 \pm 2.2 \text{ ps}(1.0 \text{ ppm}), \quad (4)$$

which is in agreement with our previous measurement [4]. The error is the quadrature average of statistical and systematic errors, where the full error matrix calculation, including all correlations, is used to combine uncertainties. The MuLan result is more than 15 times as precise as any other individual measurement [5,11] and consequently dominates the world average. Our result lies 2.5σ below the current PDG average [12]. Figure 2 shows the recent history of measurements, together with the MuLan average.

Our value for τ_{μ^+} leads to the most precise determination of the Fermi constant:

$$G_F(\mathrm{MuLan}) = 1.166\,378\,8(7) \times 10^{-5} \text{ GeV}^{-2}(0.6 \text{ ppm}). \quad (5)$$

The positive muon lifetime is also used to obtain ordinary muon capture rates in hydrogen [13] or deuterium [14] by the lifetime difference method: $\Gamma_{\mathrm{cap}} = 1/\tau_{\mu^-} - 1/\tau_{\mu^+}$. These capture rates determine hadronic quantities as discussed in Ref. [15]. For example, our new result lowers the $\mu^- p$ capture rate used in Ref. [13] by 8 s^{-1} and thus shifts g_P upward to even better agreement with theory. Finally, the improved precision reduces the τ_{μ^+} uncertainty in the determination of muon capture in Ref. [13] and future efforts to below 0.5 s^{-1}.

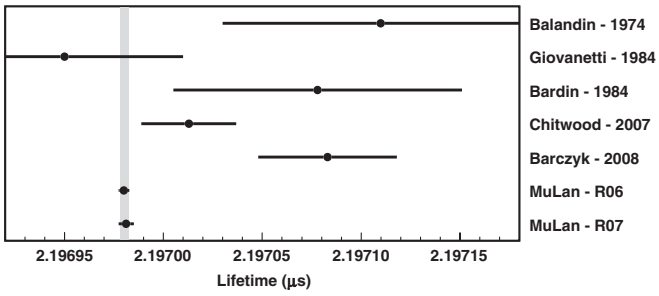

FIG. 2. Lifetime measurement summary. The MuLan R06 and R07 results are plotted separately to illustrate the consistency. The vertical shaded band is centered on the MuLan weighted average with a width equal to the combined uncertainty.

We thank the PSI staff, especially D. Renker, K. Deiters, M. Hildebrandt, R. Scheuermann, and A. Stoykov; M. Barnes and G. Wait from TRIUMF for the kicker design; the NCSA for enabling and supporting the data analysis effort; and the U.S. National Science Foundation for their financial support.

[1] S. M. Berman, Phys. Rev. **112**, 267 (1958); T. Kinoshita and A. Sirlin, Phys. Rev. **113**, 1652 (1959); S. M. Berman and A. Sirlin, Ann. Phys. (N.Y.) **20**, 20 (1962).
[2] W. J. Marciano, Phys. Rev. D **60**, 093006 (1999).
[3] T. van Ritbergen and R. G. Stuart, Nucl. Phys. **B564**, 343 (2000); Phys. Lett. B **437**, 201 (1998); Phys. Rev. Lett. **82**, 488 (1999).
[4] D. B. Chitwood *et al.* (MuLan Collaboration), Phys. Rev. Lett. **99**, 032001 (2007).
[5] A. Barczyk *et al.* (FAST Collaboration), Phys. Lett. B **663**, 172 (2008).
[6] Alexey Pak and Andrzej Czarnecki, Phys. Rev. Lett. **100**, 241807 (2008).
[7] M. J. Barnes and G. D. Wait, IEEE Trans. Plasma Sci. **32**, 1932 (2004); R. B. Armenta, M. J. Barnes, and G. D. Wait, in *Proceedings of the 15th IEEE International Pulsed Power Conference, Monterey, 2005* (IEEE, New York, 2005).
[8] Arnokrome™ III (AK-3) is an alloy of ≈ 30% Cr, ≈ 10% Co, and ≈ 60% Fe. Arnold Engineering Co., Alnico Products Division, 300 N. West Street, Marengo, IL 60152, USA.
[9] J. H. Brewer *et al.*, Physica (Amsterdam) **289B–290B**, 425 (2000).
[10] Andrzej Czarnecki, G. Peter Lepage, and William J. Marciano, Phys. Rev. D **61**, 073001 (2000).
[11] G. Bardin *et al.*, Phys. Lett. **137B**, 135 (1984); K. Giovanetti *et al.*, Phys. Rev. D **29**, 343 (1984); M. P. Balandin *et al.*, Zh. Eksp. Teor. Fiz. **40**, 811 (1974); J. Duclos *et al.*, Phys. Lett. **47B**, 491 (1973).
[12] C. Amsler *et al.* (Particle Data Group), Phys. Lett. B **667**, 1 (2008), and partial update for the 2010 edition.
[13] V. A. Andreev *et al.* (MuCap Collaboration), Phys. Rev. Lett. **99**, 032002 (2007).
[14] V. A. Andreev *et al.* (MuSun Collaboration), arXiv:1004.1754.
[15] Peter Kammel and Kuniharu Kubodera, Annu. Rev. Nucl. Part. Sci. **60**, 327 (2010).